US. Controlled prospective studies using more standardized imaging interpretation criteria may be necessary for further analysis. Secondly, collateral circulation was not evaluated by US due to the above-mentioned reasons, which might affect the results, too. Thirdly, the majority of the LC patients had compensated LC with good liver function, and the major causes of CH and LC were hepatitis C or hepatitis B viral infection; decompensated cirrhosis and cirrhosis due to other causes may have different features. Finally, there was considerable overlap between CH and compensated cirrhosis; however, disease progression from CH to LC was continuous, which rendered it difficult to precisely distinguish between these two conditions. Furthermore, identification of the transitional stage (or P-LC) remains a great challenge for the imaging techniques. Further advances in US, CT and MRI and the development of new contrast agents and radiopharmaceuticals should lead to improved imaging accuracy for LC in the future [5].

In conclusion, US, CT and MRI had different independent predictive signs for the diagnosis of LC including irregular and nodular liver surface, blunt liver edge, liver morphological changes for US, and liver parenchymal abnormalities, manifestations of portal hypertension and liver morphological changes for MRI and CT (in addition to irregular or nodular liver surface). ROC analysis showed that MRI, CT and US did not statistically differ in predicting cirrhosis. These cross-sectional imaging techniques play an important role in the noninvasive diagnosis of cirrhosis. Most interestingly, 50% of the P-LC cases were identified as LC by imaging, suggesting that P-LC should be regarded as early-stage LC in terms of fibrosis, circulatory disturbance and incidence of HCC. Therefore, imaging modalities play a very important role in the noninvasive diagnosis of histologically proven P-LC.

Disclosure Statement

The authors declare that they have no financial conflict of interest.

References

1 Anthony PP, Ishak K, Nayak NC, et al: The morphology of cirrhosis. Recommendations on definition, nomenclature, and classification by a working group sponsored by the World Health Organization. J Clin Pathol 1978;31:395–414.

2 Saunders JB, Walters JRF, Davies P, et al: A 20-year prospective study of cirrhosis. Br Med J 1981;282:263–266.

3 Fattovich G, Giustina G, Degos F, et al: Morbidity and mortality in compensated cirrhosis type C: a retrospective follow-up study of 384 patients. Gastroenterology 1997;112:463–472.

4 Ito K, Mitchell DG, Hann FW, et al: Compensated cirrhosis due to viral hepatitis: Using MR imaging to predict clinical progression. AJR 1997;169:801–805.

5 Brown JJ, Naylor MJ, Yagan N: Imaging of hepatic cirrhosis. Radiology 1997;202:1–16.

6 Rofsky NM, Fleishaker H: CT and MRI of diffuse liver disease. Semin Ultrasound CT MRI 1995;16:16–33.

7 Murakami T, Mochizuki K, Nakamura H: Imaging evaluation of the cirrhotic liver. Semin Liver Dis 2001;21:213–224.

8 Harbin WP, Rober NJ, Ferrucci JT Jr: Diagnosis of cirrhosis based on regional changes in hepatic morphology: a radiological and pathological analysis. Radiology 1980;135:273–283.

9 DiLelio A, Cestari C, Lomazzi A, et al: Cirrhosis: diagnosis with sonographic study of the liver surface. Radiology 1989;172:389–392.

10 Hess CF, Schmiedl U, Koelbel G, et al: Diagnosis of liver cirrhosis with US: receiver-operating characteristic analysis of multidimensional caudate lobe indexes. Radiology 1989;171:349–351.

11 Vilgrain V, Lebrec D, Menu Y, et al: Comparison between ultrasonographic signs and the degree of portal hypertension in patients with cirrhosis. Gastrointest Radiol 1990;15:218–222.

12 Torres WE, Whitmire LF, Gedgaudas-McClees K, et al: Computed tomography of hepatic morphologic changes in cirrhosis of the liver. J Comput Assist Tomogr 1986;11:47–50.

13 Honda H, Onitsuka H, Masuda K, et al: Chronic liver disease: value of volumetry of liver and spleen with computed tomography. Radiat Med 1990;8:222–226.

14 Itai Y, Kurosaki Y, Saida Y, et al: CT and MRI in detection of intrahepatic portosystemic shunts in patients with liver cirrhosis. J Comput Assist Tomogr 1994;18:768–773.

15 Goldberg HI, Moss AA, Stark DD, et al: Hepatic cirrhosis: magnetic resonance imaging. Radiology 1984;153:737–739.

16 Ito K, Mitchell DG, Gabata T, et al: Viral-induced cirrhosis: grading of severity using MR imaging. AJR 1999;173:591–596.

17 Gaiani S, Gramantieri L, Venturoli N, et al: What is the criterion for differentiating chronic hepatitis from compensated cirrhosis? A prospective study comparing ultrasonography and percutaneous liver biopsy. J Hepatol 1997;27:979–985.

18 Aube C, Oberti F, Korali N, et al: Ultrasonographic diagnosis of hepatic fibrosis or cirrhosis. J Hepatol 1999;30:472–478.

19 Waller RM III, Oliver TW Jr, McCain AH, et al: Computed tomography and sonography of hepatic cirrhosis and portal hypertension. Radiographics 1984;4:677–714.

20 Murakami T, Nakamura H, Hori S, et al: CT and MRI of cirrhotic regenerating nodules in hepatic cirrhosis. J Comput Assist Tomgr 1992;16:578–582.

21 Ito K, Mitchell DG, Gabata T: Enlargement of hilar periportal space: a sign of early cirrhosis at MR imaging. J Magn Reson Imaging 2000;11:136–140.

22 Pugh RN, Murray-Lyon IM, Dawson JL, et al: Transection of the oesophagus for bleeding oesophageal varices. Br J Surg 1983;60:646–649.

23 Infante-Rivard C, Esnaola S, Villeneuve JP: Clinical and statistical validity of conventional prognostic factors in predicting short-term survival among cirrhotics. Hepatology 1987;7:660–664.
24 Desmet VJ, Gerber M, Hoofnagle JH, et al: Classification of chronic hepatitis: diagnosis, grading and staging. Hepatology 1994; 19:1513–1520.
25 Swets JA: Measuring the accuracy of diagnostic systems. Science 1988;240:1285–1293.
26 Giorgio A, Amoroso P, Lettieri G, et al: Cirrhosis: value of caudate to right lobe ratio in diagnosis with US. Radiology 1986;161:443–445.
27 Goyal AK, Pokharna DS, Sharma SK: Ultrasonic diagnosis of cirrhosis: reference to quantitative measurements of hepatic dimensions. Gastrointest Radiol 1990;15:32–34.
28 Ohtomo K, Itai Y, Ohtomo Y, et al: Regenerating nodules of liver cirrhosis: MR imaging with pathologic correlation. AJR 1990;154: 505–507.
29 Shah SH, Hayes PC, Allan PL, et al: Measurement of spleen size and its relation to hypersplenism and portal hemodynamics in portal hypertension due to hepatic cirrhosis. Am J Gastroenterol 1996;91:2580–2583.
30 Ito K, Mitchell DG, Gabata T, et al: Expanded gallbladder fossa: simple MR imaging sign of cirrhosis. Radiology 1999;211:723–726.
31 Venbrux AC, Friedman AC: Diffuse hepatocellular diseases, portal hypertension, and vascular diseases; in Friedman AC, Dachman AH (eds): Radiology of the Liver, Biliary Tract, and Pancreas. St. Louis, Mosby Year Book, 1994, pp 49–168.
32 Itai Y, Ohnishi S, Ohtomo K, et al: Regenerating nodules of liver cirrhosis: MR imaging with pathologic correlation. AJR 1987;165: 578–582.
33 McCain AH, Bernardino ME, Sones PJ Jr, et al: Varices from portal hypertension: correlation of CT and angiography. Radiology 1985;154:63–69.
34 Tissot O, Aube C, Namour A, et al: Semiologie echographique de la cirrhose: concordance inter-observateur. Gastroenterol Clin Biol 1995;19:291–296.
35 Menu Y: Modern imaging of the liver and biliary tract; in McIntyre N, Benhamou JP, Bircher J, Rizzetto M, Rodes J (eds): Oxford Textbook of Clinical Hepatology. New York, Oxford Medical, 1991, pp 326–343.
36 Tanaka S, Kitamura T, Nakanishi K, et al: Recent advances in ultrasonographic diagnosis of hepatocellular carcinoma. Cancer 1989;63:1313–1317.
37 Maharaj B, Maharaj RJ, Leary WP, et al: Sampling variability and its influence on the diagnostic yield of percutaneous needle biopsy of the liver. Lancet 1986;1:523–525.
38 Nord JH: Biopsy diagnosis of cirrhosis: blind percutaneous versus guided direct vision techniques. A review. Gastrointest Endosc 1982;28:102–104.
39 Lee R: Fibrosis and cirrhosis; in Lee RG (ed): Diagnostic Liver Pathology. St. Louis, Mosby, 1994, pp 281–308.
40 Chevallier M, Guerret S, Chossegros P, et al: A histological semiquantitative scoring system for evaluation of hepatic fibrosis in needle liver biopsy specimens: comparison with morphometric studies. Hepatology 1994;20: 349–355.
41 Takano S, Yokosuka O, Imazeki F, et al: Incidence of hepatocellular carcinoma in chronic hepatitis B and C: a prospective study of 251 patients. Hepatology 1995;21:650–655.

●肝脂肪沈着の臨床

Non-alcoholic Fatty Liver Disease (NAFLD)の造影超音波診断*

飯島 尋子[1)] 斉藤 正紀[1)] 吉川 昌平[1)] 東浦 晶子[2)] 脇 英彦[2)]
森安 史典[3)] 西口 修平[1)]

Key Words：非アルコール性脂肪性肝炎(NASH)，超音波診断，画像診断，脂肪肝

要旨

Non-alcoholic steatohepatitis(NASH)の診断は，これまで画像検査では診断が不可能とされ，組織学的検査で診断されている．Sonazoid®やLevovist®は肝臓のKupffer細胞に貪食される機能を有するが，この機能を利用した造影超音波検査によるNASHの診断は，日常の診療の中で，多くの脂肪肝患者の中から線維化が進行するNASHを拾い上げることができる．

肝胆膵画像 2008：10：53-57

■はじめに

Non-alcoholic steatohepatitis(NASH)は日常診療において比較的よく遭遇する疾患で，アルコール性肝障害，ウイルス性肝炎，薬剤性肝障害，自己免疫性肝疾患を否定できる肝炎の多くがこの疾患であると思われる．

特に最近，食生活の欧米化に伴い肥満の人口が増加しNASHの存在概念が注目されている．ことに肥満症は，糖尿病，高血圧症，高脂血症，脂肪肝などの生活習慣病を伴いやすい．つい最近まで，脂肪肝は，食事療法と運動療法などで改善する可逆性の疾患と考えられてきた．

NASHの診断は，これまで画像検査では診断が不可能とされ，組織学的診断によって行われている[1)]．したがって単純に脂肪肝と診断され，線維化が進行した状態で発見されていたことも多いと推測する．

筆者らは，以前から，経静脈性超音波造影剤を用いて肝腫瘍診断や肝機能診断への応用について基礎的，臨床的検討を行ってきた．Levovist®造影超音波検査による肝腫瘍診断は，ほぼ確立されている．本稿では，Levovist®を使用したNASH診断の有用性を造影超音波検査の概略とあわせて紹介する．

■脂肪肝，NASHの画像診断

NASHを含む肝臓への脂肪浸潤の画像診断は，従来から超音波所見でbright liver, high-level echo, hepato-renal contrast, vascular blurring, deep attenuationなどと報告されている[2,3)]．しかし客観性に欠けるためCTでの検査が用いられている．つまり，肝脾のCT値をとりその比を求める方法が一般的で多く用いられていると思われる[4)]．肝脾CT値比(L/S比)0.9未満の時に脂肪肝と診断できる(図1)．またMRI検査においては，in phaseで，肝の信号は，脾臓と比較して高信号であり，opposed phaseでは，肝の信号が低下している(図2a，b)．しかし，これらの方法により，脂肪肝の診断は可能であるが，NASHとの鑑別診断は不可能である．

* Diagnosis of NASH Using Contrast Ultrasound with Levovist
1) 兵庫医科大学 内科 肝胆膵科(〒663-8501 兵庫県西宮市武庫川町1-1) Hiroko IIJIMA, Masaki SAITO, Shohei YOSHIKAWA, Syuhei NISIGUCHI : Hepat-Biliary Pancreatic Medicin, Hyogo College of Medicine, *Nishinomiya*
2) 同超音波センター Akiko HIGASHIURA, Hidehiko WAKI : Ultrasound Imaging Center, Hyogo College of Medicine, *Nishinomiya*
3) 東京医科大学 消化器内科 Fuminori MORIYASU : Department of Gastroenterology and Hepatology, Tokyo Medical University, *Tokyo*

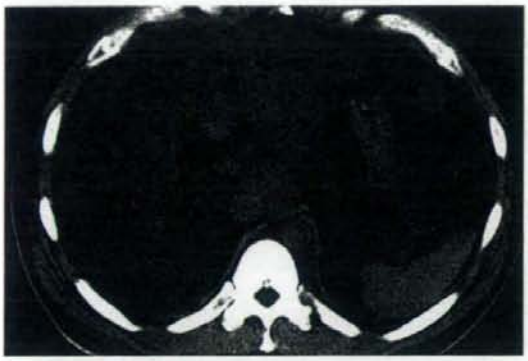

図1 脂肪肝症例のCT画像
肝／脾0.3であり，CTで脂肪肝と診断できる．

一般人口におけるNASHの発症頻度は不明であるが，北米では，肝障害で肝生検をした症例の7～10%にNASHを認めたと報告[5,6]され，スクリーニングでnonalcoholic fatty liver disease(NAFLD)のすべての患者に肝生検を施行するのは現実的でない．わが国での発症頻度に関する報告は不明であるが，検診者の8%がNAFLDで，その10%がNASHであると報告されている[7]．上記のごとく，従来の超音波B-モード，CT，MRIでも通常の脂肪肝とNASHの鑑別は困難であるが，NASHの約30%が肝硬変に進展しており，現時点では，多くのNAFLDから効率よく的確にNASHを拾い上げることが重要である．

■造影超音波検査とは

CTやMRIでは造影剤を使用した診断が，ごく当たり前に外来で行われている．しかし，造影超音波診断は，1980年代にMatsudaらにより行われたCO_2動注による方法が初めてである．その後Levovist®が保険適応になり，10年が経過したが，その使用はまだ特別な感がある．しかしその質的診断，治療への応用などは，めまぐるしく進歩，発展している[8~10]．

超音波造影剤は数種類あるが，バブルの性質から大きく分けると，vascular phaseだけ持ち，類洞，Kupfferイメージを持たないもの(Definity®, SonoVue®)と，delayed parenchymal phase(Kupffer イメージ)を持つもの(Levovist®, Sonazoid®)がある．肝臓の機能診断には，Kupfferイメージを得ることが重要であり，造影剤として，現在わが国で使用できるのはLevovist®とSonazoid®がある．次世代造影剤Sonazoid®は，中低音圧で使用できるためLevovist®より簡単に造影効果が得られる．しかもvascular，Kupfferイメージの両方を持っており肝臓の腫瘍診断のみならず機能診断にも使用できる有用性が高い造影剤と考えている．しかし，現在のところ適応が取れておらず機能診断に適切な投与量や投与方法なども確立されていない．今後の検討課題である．

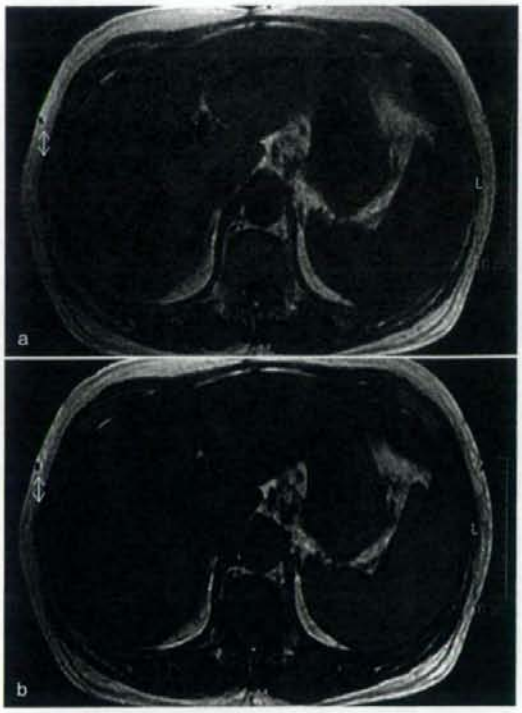

図2 脂肪肝症例のMRI画像
a. in phase, b. out of phase.

■超音波造影剤Levovist®の映像法

微小気泡から成る多くの超音波造影剤は，超音波の照射を受けると容易に共振・崩壊する．気泡の共振・崩壊の際の信号を映像化するには，組織からの

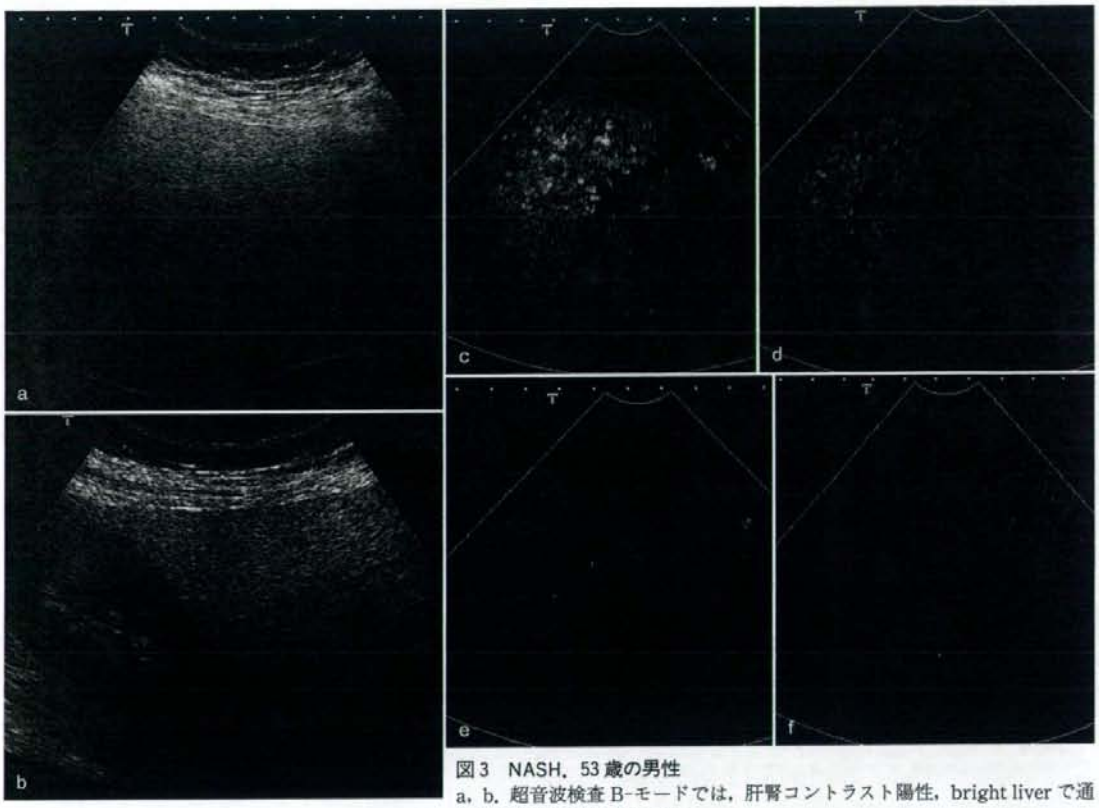

図3　NASH，53歳の男性
a，b．超音波検査B-モードでは，肝腎コントラスト陽性，bright liverで通常の脂肪肝と鑑別できない．
c～f．肝実質へのLevovist®の取り込みは，投与後5分から低下しており，15分の時点では，取り込みをほとんど認めない．
c．5分後，d．10分後，e．15分後，f．50分後．

信号を抑え，気泡からの信号を映像化することが必要である．

ここ数年，Levovist®に特化した映像手法が多く開発された．高音圧で送信し，かつ造影感度を向上させるために，複数回のパルスを送信し，受信パルス波の相関から気泡信号を抽出するなどの手法である．従来のドプラ法とは異なり，非線形信号をより多く取り出す方法が採用される．これらは，Levovist®に対する感度や空間分解能に優れている．

検討に使用した超音波装置は，東芝Aplio（東芝メディカルシステム，東京）である．プローブは，コンベックス型，中心周波数は，3.75 MHzを使用し，Levovist®に適した造影モードであるAdvanced Dynamic Flow（ADF）にて撮影を行った．Mechanical index（MI）は，1.6を使用し，フォーカスは，体表から深さ5 cmに設定した．Levovist®をbolus静注後5～20分で，スキャン断面を変えて肝臓をスキャンし，Levovist®のバブルからの信号のみを分離してシグナルの輝度を測定した．

■撮影方法の実際

筆者らは，Levovist®の肝臓における造影超音波検査における時相の名称について以前より検討し報告してきた[11]．肝実質では，投与後5分に最高輝度を示し，投与後20分までplateauを示した．この時相を，肝実質遅延相（delayed parenchymal phase）と呼ぶ．健常成人では，delayed parenchymal phase

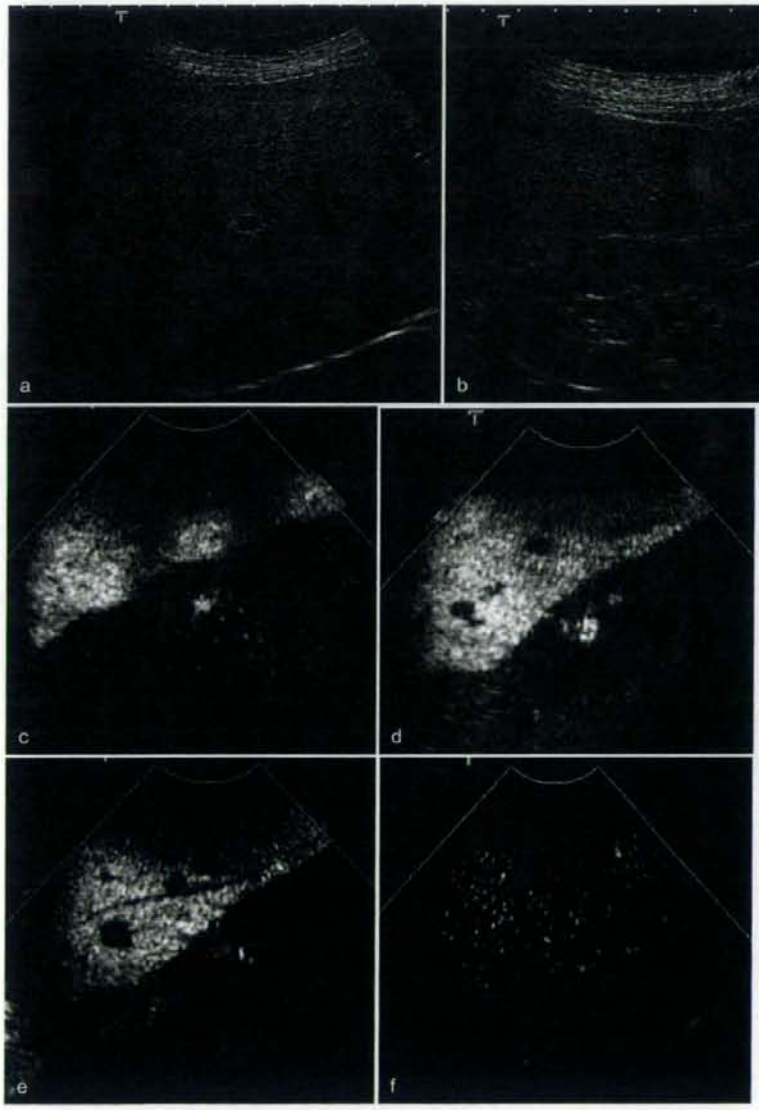

図4　脂肪肝，62歳男性
a，b．超音波検査　B-モードでは，深部減衰，肝腎コントラスト陽性を示す．
c～f．肝実質へのLevovistの取り込みは，5～15分まではプラトーで，50分かけて徐々に染影は低下する．
c．5分後，d．10分後，e．15分後，f．50分後．

の染影輝度は，約5分でピークに達し，約20分間ピークが続く．その後約50分かけて徐々に消失する．約20分後では，造影剤は血管内にほとんどなく，肝臓においてはマクロファージであるKupffer細胞に貪食されている．

以上の検討結果から，びまん性肝疾患の実質染影に関しては，5～20分の間の染影の観察が最も重要であると考えている．

■症例

NASHと脂肪肝の症例を呈示する．53歳の男性．全身倦怠感と肝機能障害で受診した．超音波B-モードでは，通常の脂肪肝と鑑別できない(図3a，b)．Levovist®を投与し，肝実質へのLevovist®の取り込みを，5～50分まで経時的に観察した．肝実質の染

影は，脂肪肝と比較して，Levovist®投与後5分から低下しており，15分の時点では，取り込みをほとんど認めない(図3c～f)．一方，組織学的に脂肪肝と診断した62歳の男性，肝機能障害で受診した．超音波B-モードでは，脂肪肝の所見である(図4a，b)．肝実質の染影は，健常人と相違なく5～15分までは，ほぼ染影はplateauであり，50分かけて徐々に染影は低下する(図4c～f)

■おわりに

マクロファージに貪食され使用できる超音波造影剤は，Levovist®とSonazoid®である．2007年1月にKupffer細胞に貪食されるように設計された造影剤であるSonazoid®が発売されたが，適応は肝腫瘍であり，肝機能診断を目的とした使用は現在のところできない．一方，Levovist®のKupffer細胞への取り込みの機序は不明であるが，肝腫瘍における臨床的検討ではすでに多くの報告がある．これらの報告では，転移性肝癌においてLevovist®のdelayed parenchymal phaseで転移部が欠損像として描出される．また，良性腫瘍と悪性腫瘍の鑑別に有用であると報告されている[12]．

肝細胞癌での検討では，SPIO-MRI(superparamagnetic iron oxide particles)とLevovist®は，ほぼ同様の染影を示したり，組織分化度との検討でも，境界病変では周囲正常肝と同様の染影を示すと報告している[13]．SPIO-MRIはすでにKupffer細胞との関連が報告されており[14]，これらの事実は，Levovist®と類洞機能，特に肝マクロファージ，Kupffer細胞による気泡の貪食能と何らかの相関が示唆される．

一方，NASHの場合，脂肪肝との大きな違いは，比較的早期からLevovist®の肝実質への取り込み低下が起こる点である[15]．このことは筆者らの経験では，線維化の程度が軽度の場合でも取り込みの低下が起こり，線維化が進行するとさらに取り込みが低下する．したがって，何らかの機序でKupffer細胞の貪食機能異常が起こっている可能性が示唆される．しかし，現在のところ，NASHの経過観察例や症例の蓄積が少なく今後の検討が待たれる．

文　献

1) Saadeh S, Younossi ZM, Remer EM, et al. The utility of radiological imaging in nonalcoholic fatty liver disease. Gastroenterology 2002 ; 123 : 745-750
2) Taylor KJ, Carpenter DA, Hill CR, et al. Gray scale ultrasound imaging. The anatomy and pathology of the liver. Radiology 1976 ; 119 : 415-423
3) 矢島義昭，太田恵，成井貴，他．脂肪肝の超音波診断肝腎コントラストの意義について．肝臓 1982 ; 23 : 903-907
4) Ricci C, Longo R, Gioulis E, et al. Noninvasive *in vivo* quantitative assessment of fat content in human liver. J Hepatol 1997 ; 27 : 108-113
5) Ludwig J, Viggiano TR, McGill DB, et al. Nonalcoholic steatohepatitis : Mayo Clinic experiences with a hitherto unnamed disease. Mayo Clin Proc 1980 ; 55 : 434-438
6) Byron D, Minuk G. Clinical hepatology : profile of an urban, hospital-based practice. Hepatology 1996 ; 24 : 813-815
7) 西原利治，小野正文，大西三朗．NASHの診断．日消誌 2004 ; 101 : 1183-1187
8) Wilson SR, Burns PN, Muradali D, et al. Harmonic hepatic US with microbubble contrast agent : initial experience showing improved characterization of hemangioma, hepatocellular carcinoma, and metastasis. Radiology 2000 ; 215 : 153-161
9) Suzuki S, Iijima H, Moriyasu F, et al. Differential diagnosis of hepatic nodules using delayed parenchymal phase imaging of levovist contrast ultrasound : comparative study with SPIO-MRI. Hepatol Res 2004 ; 29 : 122-126
10) Shimizu M, Iijima H, Horibe T, et al. Usefulness of contrast-enhanced ultrasonography with a new contrast mode, Agent Detection Imaging, in evaluating therapeutic response in hepatocellular carcinoma treated with radio-frequency ablation therapy. Hepatol Res 2004 ; 29 : 235-232
11) 飯島尋子，森安史典．造影超音波検査法の時相—肝腫瘍のKupffer imagingについて．映像情報 2002 ; 34 : 75-79
12) Albrecht T, Blomley MJ, Burns PN, et al. Improved detection of hepatic metastases with pulse-inversion US during the liver-specific phase of SHU 508 A : multicenter study. Radiology 2003 ; 227 : 361-370
13) Suzuki Y, Fujimoto Y, Hosoki Y, et al. Clinical utility of sequential imaging of hepatocellular carcinoma by contrast-enhanced power Doppler ultrasonograpy. Eur J Radiol 2003 ; 48 : 214-219
14) Takeshita K, Nagashima I, Frui S, et al. Effect of superparamagnetic iron oxide-enhanced MRI of the liver with hepatocellular carcinoma and hyperplastic nodule. J Comput Assist Tomogr 2002 ; 26 : 451-455
15) Moriyasu F, Iijima H, Tsuchiya K, et al. Diagnosis of NASH using delayed parenchymal imaging of contrast ultrasound. Hepatol Res 2005 ; 33 : 97-99

DATA ANALYSIS 4

NAFLD(非アルコール性脂肪性肝疾患)の線維化スコア：NAFLDの非侵襲的線維化スコアリングシステムの検討

NAFLDの治療において肝線維化の進行度判定は重要であり，本論文は，臨床・血液データから非侵襲的かつ簡便に行う診断法について検討，スコアリングシステムを考案し，肝生検症例を用いてそれを検証している。

表1 Predictive Value of the Scoring System Obtained from the Estimation Group (n=480)

	Low cutoff point (<-1.455)	Indeterminate (-1.455-0.676)	High cutoff point (>0.676)	Total
Total	295	114	71	480
NO significant fibrosis (stage 0-2)	273	75	7	355
Significant fibrosis (stage 3-4)	22	39	64	125
Sensitivity	82 %		51 %	
Specificity	77 %		98 %	
Positive predictive value	56 %		90 %	
Negative predictive value	93 %		85 %	
Likelihood ratio (+)	3.567		25.966	
Likelihood ratio (-)	0.229		0.498	
Interpretation	Absence of significant fibrosis (93 % certainty)		Presence of significant fibrosis (90 % certainty)	

NOTE. Prevalence of advanced fibrosis of 26 % in the estimation group.
カットオフ値を-1.455以下とすると355例中273例(77 %)がfibrosis stage 0-2と診断されnegative predictive valueは93 %であった。カットオフ値を0.676以上とすると125例中64例(50 %)がfibrosis stage 3-4の高度線維化と診断された。Positive predictive valueは90 %であった。

肥満，Ⅱ型糖尿病，メタボリックシンドロームの増加に伴い非アルコール性脂肪性疾患(NAFLD)が増加している。NAFLD は肝硬変，肝不全あるいは HCC に進行しうることから，肝線維化の進行度の正確な診断が求められる。肝線維化の診断には肝生検が最も正確とされるが，侵襲性が高く，合併症を伴うこともあり肝生検組織のサンプリングエラーも起こりうる。本論文では臨床，血液データを用いることにより，①NAFLD の肝線維化の重症度判定のためのスコアリングシステムの作成および②そのシステムの検証を多施設共同試験で行った。肝生検で NAFLD と診断された 4 ヵ国 4 施設の患者計 733 人をスコアリングシステム作成グループ(480 患者)，スコアリングシステム検証グループ(253 患者)の 2 群に分けた。特に，Kleiner らが改訂した Blunt の分類の fibrosis stage 3-4 の線維化の鑑別を目的とした。

多変量解析により高度の線維化の有無に関連する変数を解析した結果，年齢，血糖値(糖尿病，高血糖)，肥満指数(BMI)，血小板数，アルブミン値，および ASL/ALT 比が肝線維化の進行度に寄与する独立因子であることが示された。これらの 6 因子を用いたスコアリングシステムとして NAFLD fibrosis score※を考案した。このシステムは，線維化の重症度判定に使用できる。NAFLD fibrosis score を用いることにより，733 患者のうち 549 患者(75 %)で肝生検せず線維化の診断ができ，496 患者(90 %)で正確に fibrosis stage 3-4 の線維化の有無を予測しえた。

NAFLD fibrosis score は，通常の血液データなどから非侵襲的かつ簡便に線維化の有無を鑑別できる点において有用であるが有効性を評価するには，さらに線維化マーカーや画像診断などを入れ線維化の正診率を向上させる必要がある。

※ NAFLD fibrosis score=−1.675+0.037×年齢(歳)+0.094×BM (kg/m²)+1.13×IFG/糖尿病の有無(有=1，無=2)+0.99×AST/ALT 比−0.013×血小板数(10^9/L)−0.66 ×アルブミン(g/dL)

兵庫医科大学内科学肝胆膵科　飯島 尋子(臨床教授)(*Iijima, Hiroko*)，西口 修平(教授)(*Nishiguchi, Shuhei*)

References

1) Ratziu V, Charlotte F, Heurtier A, et al : Sampling variability of liver biopsy in nonalcoholic fatty liver disease. Gastroenterology 128 : 1898-1906, 2005

2) Rousselet MC, Michalak S, Dupre F, et al : Source of variability in histological scoring of chronic viral hepatitis. Hepatology 41 : 257-264, 2005

The American Journal of Pathology, Vol. 173, No. 3, September 2008

DOI: 10.2353/ajpath.2008.071091

Tumorigenesis and Neoplastic Progression

G-Protein-Coupled Receptor GPR49 is Up-regulated in Basal Cell Carcinoma and Promotes Cell Proliferation and Tumor Formation

Keiji Tanese,*† Mariko Fukuma,* Taketo Yamada,* Taisuke Mori,* Tsutomu Yoshikawa,‡ Wakako Watanabe,‡ Akira Ishiko,† Masayuki Amagai,† Takeji Nishikawa,† and Michiie Sakamoto*

From the Department of Pathology and Department of Dermatology,† School of Medicine, Keio University, Tokyo, Japan; Discovery Technology Laboratory,‡ Pharmaceuticals Research Division, Mitsubishi Pharma Corporation, Yokohama, Japan*

The significance of Hedgehog (HH) signaling in the development of basal cell carcinoma (BCC) has been established. Although several target genes of HH signaling have been described previously, their precise role in tumorigenesis and cell proliferation is not yet known. To identify genes responsible for tumor formation in BCC, we screened a DNA microarray database of human BCC cases; the orphan G-protein-coupled receptor GPR49 was found to be up-regulated in all cases. GPR49 is a novel gene reported to be a marker of follicular and other tissue stem cells. Using real-time quantitative RT-PCR analysis, significant expression of GPR49 mRNA was observed in 19 of 20 BCC cases (95%) compared with controls. Up-regulation of GPR49 was confirmed by *in situ* hybridization. Moreover, knockdown of mouse Gpr49 showed suppression of cell proliferation in a mouse BCC cell line, and overexpression of GPR49 in human immortalized keratinocyte HaCaT cells induced proliferation. Furthermore, HaCaT cells overexpressing GPR49 showed tumor formation when transplanted into immunodeficient mice. In addition, inhibition of the HH signaling pathway in a mouse BCC cell line down-regulated endogenous Gpr49, whereas activation of HH signaling in mouse NIH3T3 cells up-regulated endogenous GPR49. These results suggest that GPR49 is expressed downstream of HH signaling and promotes cell proliferation and tumor formation in cases of BCC. *(Am J Pathol 2008, 173:835–843; DOI: 10.2353/ajpath.2008.071091)*

Basal cell carcinoma (BCC) is a common malignant tumor of the skin. Histopathologically, they usually arise from the lowermost layers of the epidermis and comprise various histological subtypes. Interestingly, BCC cells have many features in common with follicular epithelium.[1]

Recent studies have shown that BCC frequently has abnormalities of the Hedgehog (HH) signaling pathway. HH signaling plays a key role in vertebrate development as it is involved in multiple biological processes such as cell differentiation, proliferation, and growth.[2] Also, several genes overexpressed in BCC have been reported to be related to HH signaling.[3] However, the genes expressed as a target of HH signaling and their functions in tumorigenesis are still not precisely understood. Further understanding of the molecules expressed in BCC and their relation between HH signaling is therefore required.

G-Protein-coupled receptor GPR49, also known as LGR5/HG38/FEX, belongs to the leucine-rich repeat containing G-protein-coupled receptors (LGRs) structurally similar to glycoprotein hormone receptors including thyroid-stimulating hormone receptor, follicle-stimulating hormone receptor, and luteinizing hormone receptor.[4] LGRs are grossly divided into three subgroups: glycoprotein hormone receptors; the subgroup of GPR48, GPR49, and LGR6; and the receptors of relaxin family ligands represented by LGR7 and LGR8.[4,5] Unlike LGRs in the other two subgroups, the ligands of GPR48, GPR49, and LGR6 have not been identified. A recent report showed that GPR49 null mice exhibited neonatal lethality characterized by ankyloglossia and gastrointestinal distension.[6] Interestingly, a recent report showed that GPR49 is expressed on stem cells in the small intestine and colon, and has also been suggested that stem

Supported by Grant-in-Aid for the 21st Century Center of Excellence program and Cancer Research from the Ministry of Education, Culture, Sports, Science and Technology of Japan; The Third Term Comprehensive 10-Year Strategy for Cancer Control from the Ministry of Health, Labor and Welfare of Japan; and research encouraging scholarship of Keio University School of Medicine.

Accepted for publication May 27, 2008.

Supplemental material for this article can be found on *http://ajp.amjpathol.org*.

Address reprint requests to Michiie Sakamoto, Department of Pathology, Keio University School of Medicine, 35 Shinanomachi, Shinjuku-ku, Tokyo 160-8582, Japan. E-mail: msakamot@sc.itc.keio.ac.jp.

Table 1. Primer Sequences for Quantitative RT-PCR

Gene	Primer orientation	Sequence
Human GAPDH	Forward	5'-CCAGCCGAGCCACATCGCTC-3'
	Reverse	5'-ATGAGCCCCAGCCTTCTCCAT-3'
Human GPR49	Forward	5'-GAGGATCTGGTGAGCCTGAGAA-3'
	Reverse	5'-CATAAGTGATGCTGGAGCTGGTAA-3'
Human GLI1	Forward	5'-GAAGACCTCTCCAGCTTGGA-3'
	Reverse	5'-GGCTGACAGTATAGGCAGAG-3'
Human GLI2	Forward	5'-TGGCCGCTTCAGATGACAGATGTTG-3'
	Reverse	5'-CGTTAGCCGAATGTCAGCCGTGAAG-3'
Mouse Gapdh	Forward	5'-TGCACCACCAACTGCTTAG-3'
	Reverse	5'-GGATGCAGGGATGATGTTT-3'
Mouse Gpr49	Forward	5'-GAGTCAACCCAAGCCTTAGTATCC-3'
	Reverse	5'-CATGGGACAAATGCAACTGAAG-3'
Mouse Gli1	Forward	5'-CATTCCACAGGACAGCTCAA-3'
	Reverse	5'-TGGCAGGGCTCTGACTAACT-3'
Mouse Ptch1	Forward	5'-CAAACTTTGACCCCTTGGAA-3'
	Reverse	5'-AAAACAAGGGGCACATCAAG-3'

cells in the hair follicle are GPR49-positive.[7] Thus, GPR49 may play a significant role in the biology of stem cells. Although the function of GPR49 in cancer is poorly understood, overexpression of GPR49 has been reported in some studies.[8,9] In particular, it is overexpressed in some hepatocellular carcinoma with β-catenin mutation and is thought to be a target of Wnt-β catenin signaling.[8]

Here we report that GPR49 is markedly up-regulated in almost all cases of BCC under the control of HH signaling, and that it plays an important role in cell proliferation and tumor formation.

Materials and Methods

Samples

Tumor samples were collected from patients at Keio University Hospital and other affiliated hospitals. Tumor and normal skin were snap-frozen after surgical removal and stored at −80°C until use. We also used paraffin-embedded sections of skin tumors. The experiment was approved by the ethics committee of Keio University School of Medicine and all samples were taken after written informed consent was obtained from the patients.

GeneChip Database and Gene Expression Analysis

The GeneChip was analyzed with the GeneExpress software system (Gene Logic Inc., Gaithersburg, MD). This database contains gene expression signatures from about 10,000 clinical samples from a variety of normal and disease conditions on the Affymetrix HG-U133 GeneChip.

DNA microarray analysis was independently performed in our laboratory with the Gene Spring Gx software system (Tomy Digital Biotechnology, Tokyo, Japan) containing gene expression signatures from four BCC and four normal skin samples on the Agilent whole human Genome oligo DNA MicroArray 4×44k (Agilene Technologies, Santa Clara, CA). For microarray hybridization, we followed the manufacturer's protocol. Difference in gene expression was quantified as the fold change in gene expression between sets of BCC-derived and normal skin tissues. Genes were considered as being differentially expressed at a significance of $P < 0.01$. We then listed the genes expressed more than six fold in BCC and hypothetical genes were eliminated.

Quantitative Real Time Polymerase Chain Reaction

Total RNA were isolated from tissues and cell lines with RNeasy Mini Kit including DNAase treatment (Quiagen KK, Tokyo, Japan). cDNA was synthesized with a First-Strand cDNA Synthesis Kit (GE Health care, Piscataway, NJ). Quantitative real time PCR (QRT-PCR) analysis was performed on an ABI7700 using SYBR Green PCR Core Reagents (Applied Biosystems, Warrington, UK). Primer sequences for QRT-PCR studies are shown in Table 1. Human and mouse GAPDH was used as a reference. Fold-induction values were calculated using the $2^{-\Delta\Delta Ct}$ method. All experiments were performed in triplicate and were repeated at least five times in separate experiments; representative data are shown.

In Situ Hybridization

Digoxigenin-labeled GPR49 sense and antisense probes were generated from the 120-bp fragment of *GPR49* (corresponding to nucleotides 2548 to 2667, GenBank NM_003667). The protocol for *in situ* hybridization is described elsewhere.[10] Briefly, de-paraffinized sections were treated with thermolysin 4 mg/ml and proteinase K 10 μg/ml, and hybridized with sense and anti-sense probes. After hybridization, the slides were washed and treated with RnaseA for 30 minutes and washed with NTE buffer (0.5M NaCl, 1 mmol/L EDTA, 10 mmol/L Tris-HCl pH 8.0) at 37°C. The sections were then washed and rinsed with NT buffer (150 mmol/L NaCl, 100 mmol/L Tris-HCl pH 7.5). Nonspecific staining was blocked with 5% normal goat serum and incubated with anti-digoxigenin-alkaline phosphatase (Roche Diagnostics, Basel,

Switzerland) diluted 1:250 in NT buffer, followed by washing. Sections were visualized by BCIP/NBT liquid substrate (0.15 mg/ml 5-bromo-4-chloro-3-indolyl phosphate solution salt, 0.3 mg/ml Nitrotetrazolium Blue Chrolide, 1 mmol/L $MgCl_2$, 100 mmol/L Tris pH 9.5).

Cell Culture and Reagents

Human immortalized keratinocyte HaCaT cells were a gift from Dr. Norbert Fusenig (German Cancer Research Center, Heidelberg, Germany). NIH3T3 cells and HaCaT cells were maintained as described elsewhere.[11] The mouse BCC cell line ASZ001 was kindly provided by Dr. Ervin Epstein (Department of Dermatology, University of California, San Francisco, CA) and Dr. Matthew P. Scott (Department of Developmental Biology, Howard Hughes Medical Institute, Stanford University School of Medicine). It was maintained as reported previously.[12] Cyclopamine (Biomol Int., Philadelphia, PA) was dissolved in 0.19% ethanol and added to ASZ001 culture at a concentration of 2 or 10 μmol/L. Purmorphamine (Calbiochem, San Diego, CA) was dissolved in dimethyl sulfoxide (Sigma-Aldrich, St. Louis, MO) and added to NIH3T3 culture at a concentration of 2 μmol/L. As a control, the same amount of 0.19% ethanol and dimethyl sulfoxide was added.

Plasmids and Transfection

Mouse Gli1 expression vector, Gli-consensus reporter gene (8×3'GBS-luc) and its mutant reporter gene (8×3'mutGBS-luc) were gifts from H. Sasaki (Riken, Kobe, Japan).[13] Human GPR49 expression vector was constructed by inserting human GPR49 full coding cDNA (RZPD, Berlin, Germany) to pcDNA3 (Invitrogen, Carlsbad, CA). Transfection was performed using Fugene6 (Roche Diagnostics, Basel, Switzerland). Expression vector-transfected cells were treated with G418 (Invitrogen) and resistant colonies were collected without cloning.

RNA Interference

RNA interference was performed using shRNA.[14] Briefly, 64- nucleotide hairpin-loop sequences (containing the 21-nucleotide shRNA targeted sequence) were generated (Sigma, Tokyo, Japan). GPR49 shRNA targeted sequences were as follows. GPR49-585: 5'-GAACAAAAUACACCACAUA-3', GPR49-662: 5'-GAAUCCACUCCCUGGGAAA-3'. As a control, we used a random 21-nucleotide sequence that does not target any known genes (B-Bridge International Inc, Mountain View, CA) to exclude a non-specific effect of the hairpins. These genes were subsequently inserted upstream of the H1RNA polymerase III promoter in a pENTR221-H1R-stuffer vector. The pENTR221 rfA cassette "expressing shRNA under the control of the human H1 promoter" was changed to the pDEST-SI-CMSCVpuro vector (CMV-based vector) using the GATEWAY system (Invitrogen) for transient transfection. pENTR221-H1R-stuffer vector and pDEST-SI-CMSCVpuro vector were provided by Dr. T. Kiyono (National Cancer Center, Tokyo, Japan). Transfected cells were treated with puromycin (Invitrogen) for 2 weeks. Puromycin-resistant colonies were collected by trypsinization and used without cloning.

Cell Proliferation Assay

Antibiotic-resistant cells were seeded in 6-well plates at 5×10^4 cells/well and incubated as described above. After seeding, cells were counted every 24 hours in a Burker-Turk counting chamber (CIS, Japan). WST-1 assay (Roche Diagnostics) and BrdU incorporation assay (Roche Diagnostics) were performed according to the manufacturer's protocol. An apotosis detection assay was performed using Annexin V-PE Apoptosis Detection Kit 1 (BD Pharmingen, San Diego, CA) and flow cytometry according to the manufacturer's protocol. All experiments were performed in triplicate and repeated separately at least five times, and representative data are shown.

Tumor Formation Assay

GPR49-overexpressed HaCaT cells and pcDNA3-transfected HaCaT cells were transplanted into NOG mice (NOD/Shi-scid/IL-2γ−/− mouse) at 1×10^7 cells without cloning. GPR49-overexpressed HaCaT cells were transplanted onto the right side of the back, and pcDNA3-transfected HaCaT cells were transplanted onto the left side. Tumor size was measured every week. Twenty-four weeks after transplantation, transplanted sites with or without tumor were resected and samples were used for histological analysis and RNA extraction. Experiments were performed in ten mice. We used mouse anti-human Ki-67 antibody (Dako, Carpinteria, CA) for Immunohistochemistry to estimate cell proliferation.

Statistical Analysis

Statistical analysis was performed using Statcel2 software (OMS, Saitama, Japan). Statistically significant differences were determined by Student's *t*-test using $P = 0.05$ as the level of significance.

Results

Overexpression of GPR49 *in BCC*

Among the genes found to be expressed in BCC from GeneChip analysis databases, GPR49 showed a significant increase compared to normal skin (Supplementary Figure S1, *http://ajp.amjpathol.org*). DNA microarray analysis in our samples also showed GPR49 expression to be about 8.3-fold higher than normal skin (Supplementary Table S1, *http://ajp.amjpathol.org*). Expression of *GPR49* was confirmed by QRT-PCR using 20 cases of BCC (Table 2) together with GLI1 and GLI2, which were reported to be overexpressed in BCC[3] and to be transcription factors involved in HH signaling. Of these 20 cases, 19 showed GPR49 expression levels more than three

Table 2. Expression Level of GPR49, GLI1, GLI2 in BCC*

Case	Pattern	Lesion	GPR49	GLI1	GLI2
Case 1	Nodular	Face	85.3	574.7	72
Case 2	Nodular	Face	78.8	664	9.5
Case 3	Nodular	Face	105.8	229.99	6.9
Case 4	Nodular	Face	234.7	726	70.8
Case 5	Nodular	Face	799.9	753.3	19.5
Case 6	Superficial	Trunk	10.6	63.54	2.3
Case 7	Nodular	Face	718.5	927	17.8
Case 8	Nodular	Face	815.6	641	12.4
Case 9	Superficial	Face	132.7	514.9	9.3
Case 10	Superficial	Trunk	1.2	5.6	0.1
Case 11	Nodular	Face	86.5	161.97	3.2
Case 12	Superficial	Trunk	53.3	410.3	15.6
Case 13	Superficial	Trunk	316.8	2362.1	96.7
Case 14	Superficial	Trunk	231.6	359.3	184.7
Case 15	Nodular	Face	90.2	512	26.6
Case 16	Nodular	Face	530.17	3983	141.6
Case 17	Nodular	Face	281.9	2101.8	30.7
Case 18	Nodular	Face	217.9	1364.4	25.9
Case 19	Nodular	Face	3219.4	7417.3	168.6
Case 20	Superficial	Trunk	1126.4	6880.3	147.27

*Each gene expression value represents the ratio of mRNA in tumor to that in normal skin mRNA.

times higher than the control (Figure 1, A and B) with a mean increase of about 450-fold). As we could not obtain a specific antibody against GPR49 suitable for immunohistochemical analysis, we performed *in situ* hybridization to determine whether tumor cells express the gene. The anti-sense signal level was higher compared to the sense probe, and the signal expression site coincided with the tumor nest in various histological subtypes (Figure 2). On the other hand, expression by QRT-PCR was low in other epidermal skin tumors (Figure 1, A and B). These results suggest that the overexpression of GPR49 is a characteristic feature of BCC.

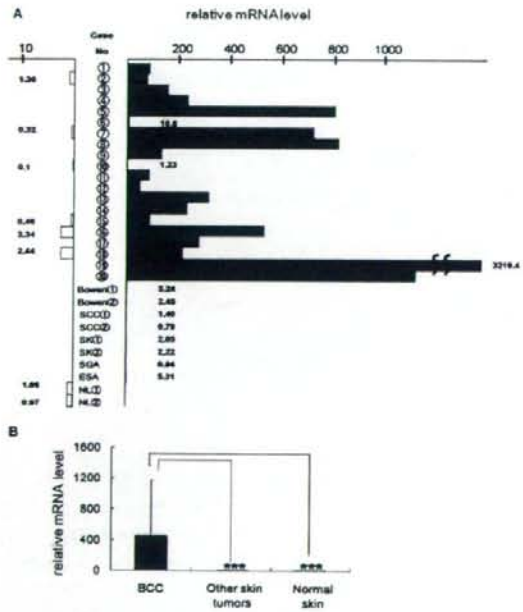

Figure 1. Expression of GPR49 in BCC. **A:** QRT-PCR of GPR49. The mRNA levels of GPR49 in 20 BCC, 8 other skin tumors, 6 normal skin in the vicinity of BCC, and 2 normal skin samples from non-cancerous patients (NL) are estimated by QRT-PCR. (Closed column: mRNA level in tumors. Open column: mRNA level in normal skin). In other types of skin tumors such as Bowen's disease, squamous cell carcinoma (SCC), sweat gland adenocarcinoma (SGA), eccrine spiradenocarcinoma (ESA), and seborrheic keratosis (SK), expression of GPR49 is negligible compared to BCC. **B:** The mean value and SD of the mRNA levels of GPR49 in BCC, other skin tumors and normal skin. About 450-fold higher levels of GPR49 are shown in BCC as compared with normal skin.

Function of GPR49 in Cell Proliferation

To identify the function of GPR49, we first performed RNA interference in BCC cell line. As no human BCC cell lines are available, we extensively tried to establish human BCC cell lines. However, we could neither obtain transplantable BCC nor establish BCC cell lines. So we used a mouse BCC cell line, ASZ001.[15] As expected, this cell line expressed mouse Gpr49 and high HH signaling activity. We constructed two sequences of shGPR49RNAi vectors (sh585 and sh662) and transfected into ASZ001 cells, and puromycin-resistant cells were collected. Knockdown experiments using sh585 and sh662 decreased GPR49 mRNA levels by 40% and 50%, respectively, compared to controls (Figure 3A) and the knockdown effect of sh585 and sh662 persisted up to day 5 after cell selection was completed. Cell growth was markedly decreased by both shGPR49RNAi vectors in comparison with the control, and suppression of cell proliferation was dependent on the knock down effect (Figure 3A). Suppression of cell proliferation was also confirmed in WST-1 and BrdU incorporation assays (data not shown). To exclude any apoptotic effect and differentiation effect of knocking down mouse *Gpr49* gene, we performed an apoptosis detection assay and analyzed the expression level of involucrin and loricrin, both of which are markers of keratinization. No significant difference was seen between control cells and mouse *Gpr49* knockdown cells (data not shown).

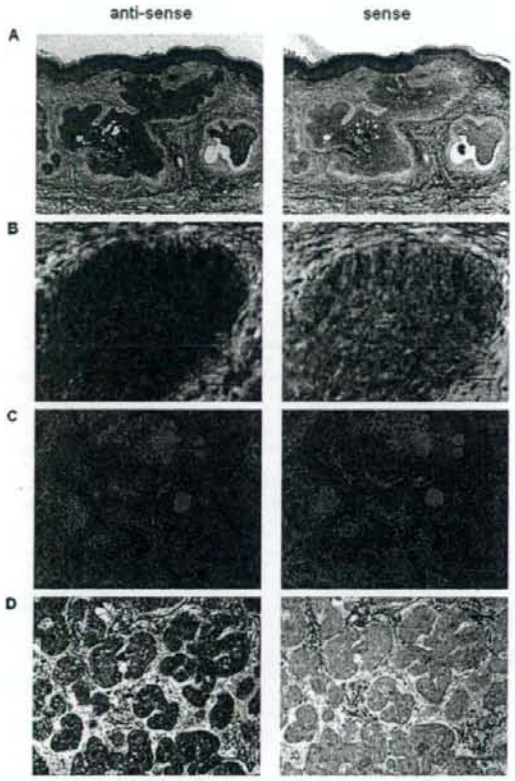

Figure 2. *In situ* hybridization of GPR49 in BCC. De-paraffinized sections were hybridized with anti-sense (left) or sense (right) probes for GPR49. **A:** Case 17. Low power view (scale bar = 1000 μm). Signal expression site hybridized with anti-sense probe coincides with the tumor nest. **B:** High magnification of case 17 (scale bar = 100 μm). Signal of anti-sense probe coincides with cytoplasm. **C:** Sclerosing type BCC (scale bar = 250 μm). **D:** Micronodular type BCC (scale bar = 250 μm).

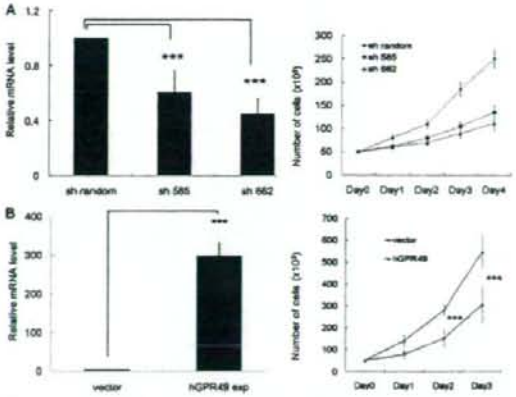

Figure 3. Function of Gpr49 in cell proliferation. **A:** Knockdown effect of shRNA against mGpr49 in ASZ001 cell proliferation. Left: Gene expression level of mouse *Gpr49* in ASZ001 harboring short-hairpin RNAi against GPR49 was measured by QRT-PCR. ASZ001 cells were transfected with shRandom, sh585 or sh662, and puromycine-resistant cells were collected for RNA extraction and cell proliferation assay. Knockdown experiments using sh585 and sh662 decreased GPR49 mRNA levels by 40% and 50%, respectively, compared to controls. Right: Cell counting. ASZ001 cells harboring shRNAi were plated on 24-well dishes (5×10^4 cells/well). Trypsinized cells were counted every 24 hours for 4 consecutive days. When the expression level of mouse Gpr49 was knocked down, cell proliferation was down-regulated in comparison with the shRandom (sh585 and sh662 to shRandom: $P < 0.01$ at day 3 and day 4). Also, down-regulation of cell proliferation was dependent on the knock down effect. **B:** The effect of overexpressing of GPR49 on cell proliferation. Left: HaCaT cells were transfected with hGPR49 expression vector, and G-418–resistant colonies were collected for RNA extraction and cell proliferation assay. The gene expression level of Gpr49 was measured by QRT-PCR. HaCaT cells harboring GPR49- expression vector showed expression of *GPR49*, about 300 times higher than cells transfected with empty vector. Right: Cell counting. HaCaT cells harboring hGPR49 expression or empty vector were plated on 24-well dishes (5×10^4 cells/well). Trypsinized cells were counted every 24 hours for 3 consecutive days. When hGPR49 is overexpressed in HaCaT cells, upregulation of cell proliferation was observed in comparison with cells transfected with empty vector. $^{***}P < 0.01$, bars = SD.

In addition, the direct effect of GPR49 expression was evaluated by transfecting human GPR49 expression vector into HaCaT cells. As we could not find or create a specific antibody against GPR49 suitable for western blotting, we performed studies using QRT-PCR. Expression of GPR49 in neomycin-resistant GPR49-transfected cells (HaCaT-GPR49exp cells) was 300 times higher than empty vector transfectants (HaCaT-vector cells), and HaCaT-GPR49exp cells showed increased cell growth (Figure 3B). Upregulation of cell proliferation was also confirmed in WST-1 assay (data not shown). In the course of cell culture, no apoptosis or cell differentiation was observed (data not shown).

Function of GPR49 in Tumor Formation

To evaluate further the function of GPR49 *in vivo*, we attempted to transplant shRNA-transfected ASZ001 cells into NOG mice, but we could not establish a stable mGpr49 knockdown ASZ001 cell culture, probably due to a growth-suppressive effect of shRNA. Then we transplanted HaCaT-GPR49exp cells into NOG mice. HaCaT cells are immortal *in vitro*, but they are also nontumorigenic and reform an orderly structured and differentiated epidermal tissue when transplanted into nude mice.[16] So we thought its normal keratinocyte-like feature of HaCaT cells would be useful to evaluate whether overexpression of GPR49 in this cell line promotes tumorigenicity. As expected, tumor formation was observed about 10 weeks after transplantation. HaCaT-vector cells also showed a cystic mass formation in three of ten mice but it did not become larger. On the other hand, HaCaT-GPR49exp cells showed tumor formation and enlargement in all mice (Figure 4A and B). Overexpression of GPR49 in the tumor of HaCaT-GPR49exp cells was confirmed to be as much as 200 times higher than HaCaT-vector cells or nodules derived from HaCaT-vector cells (Figure 4C). In histological examination, nodules of empty vector transfected cells showed a small cystic structure containing keratinizing material and calcification. The cyst wall was composed of a thin and uniform epithelial structure (Figure 4D). On the other hand, the solid tumor made from HaCaT-GPR49exp cells displayed dyskeratosis, cancer pearls with a high tendency toward proliferation and interstitial invasion. Cell proliferation of the tumor made

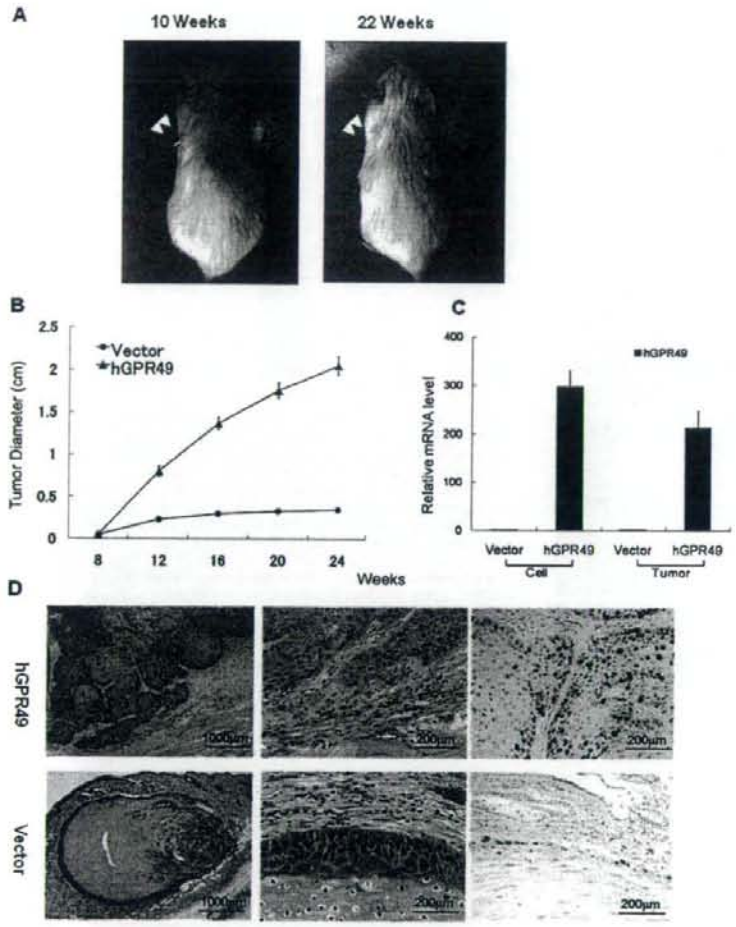

Figure 4. hGPR49-overexpressed HaCaT cells showed tumor formation in NOG mice. **A:** Tumor formation at 10 weeks (left panel) and 22 weeks (right panel). HaCaT cells overexpressing hGPR49 (1×10^7 cells) were transplanted subcutaneously on the back of NOG mice on the right side. Cells with empty vector were also transplanted onto the back of the same mouse on the left side. Cells with hGPR49 formed tumors (closed **arrows**) in all ten mice, while only a nodule (open **arrowheads**) was formed in three mice with cells harboring empty vector. **B:** Measurement of tumor size. The diameters of tumors were measured every other week after transplantation. Apparent tumor formation was observed 10 weeks after transplantation. All ten tumors derived from GPR49-overexpressed cells continued to grow until 24 weeks, while three nodules derived from cells with empty vector did not show enlargement. **C:** Gene expression level of *GPR49* in innoculated cells and in formed tumors was measured by QRT-PCR. Tumors derived from GPR49-overexpressed HaCaT cells showed high levels of hGPR49, about 200 times higher than the nodule with empty vector (bars = SD). **D:** Histological examination. Tumors derived from GPR49-overexpressed HaCaT cells showed aberrant proliferation and invasion. Keratinization was observed in some tumor nests and had features resembling squamous cell carcinoma (upper panels). The nodule derived from HaCaT cells with empty vector showed a cystic structure with keratinization and calcification (lower panels). Left panels: low magnification (scale bar = 1000 μm), Middle panels: high magnification (scale bar = 200 μm). Right panels: immunohistochemical staining of Ki-67. Significantly increased expression of Ki-67 coincident with nucleus is observed in tumors derived from GPR49-overexpressed HaCaT cells (scale bar = 200 μm).

from HaCaT-GPR49exp cells was examined by Ki-67 immunohistochemical staining, and HaCaT-GPR49exp cells showed significantly increased expression of Ki-67 (Figure 4D). These findings indicate that GPR49 promotes cell proliferation and tumor formation.

Relation between GPR49 and HH Signaling

Using 20 cases of BCC, expression of GPR49, GLI1 and GLI2 was confirmed by QRT-PCR as listed in Table 2. So we analyzed the correlation between the expression level of GPR49 and GLI1, GLI2 to evaluate the relation between HH signaling and GPR49. Statistical analysis using Pearson's coefficient was calculated for all combinations. A high correlation was seen between the expression levels of GPR49 and GLI1 at $r = 0.802$. Also, a mild correlation was observed between GPR49 and GLI2 ($r = 0.539$), GLI1 and GLI2 ($r = 0.707$) (Table 3). As HH signaling is activated in BCC, we speculated here that expression of GPR49 is highly related to HH signaling.

To further evaluate the relation between HH signaling and GPR49, we performed an *in vitro* assay using cell lines. Activation and suppression of HH signaling was confirmed by the reporter constructs of HH signaling.[13] Luciferase activity of 8×3'GBS-luc is much higher than 8×3'mutGBS-luc in the condition of activated HH signaling. (Supplementary Figure S1, *http://ajp.amjpathol.org*). We treated ASZ001 with cyclopamine, a known inhibitor of HH signaling. Down-regulation of mouse Gpr49 expression was observed together with down-regulation of

Table 3. Pearson Coefficient Analysis of Each Gene Expressed in BCC**

	GPR49	GLI1	GLI2
GPR49		0.804424	0.539395
GLI1	0.804424		0.707205
GLI2	0.539395	0.707205	

**Pearson correlation coefficient (two-tailed) was calculated pairwise using Statcel2 software for all combinations. ($P < 0.01$)

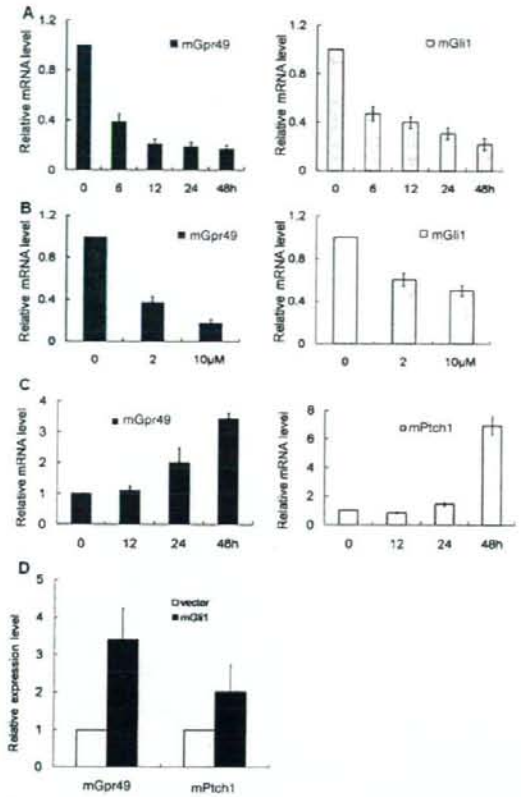

Figure 5. HH signaling regulates Gpr49 expression. **A:** Time course of mRNA expression of endogenous mGpr49 and mGli1 in ASZ001 cells treated with cyclopamine. Cells were treated with 10 μmol/L of cyclopamine, and expression of mGpr49 (left) and mGli1 (right) mRNA was measured by QRT-PCR at the times shown in the figure. The fold decrease of mRNA levels in cyclopamine-treated to non-treated cells at each sampling time was normalized setting the baseline value at 1. The figure is one of the five repeated experiments. Suppression of mGpr49 and mGli1 expression was dependent on the time course. The expression level of mGpr49 was persistently decreased by 20% of initial time in 48 hours after treatment. Statistical analysis using Pearson's coefficient was calculated for each time's combination and a high correlation was seen between the expression levels of mGpr49 and mGli1 at $r = 0.985$ ($P < 0.01$). **B:** Dose dependency of mRNA expression of mGpr49 and mGli1 on the concentration of cyclopamine. ASZ001 cells were treated with 0, 2, and 10 μmol/L of cyclopamine, and expression of mGpr49 (left) and mGli1 (right) was measured by QRT-PCR 48 hours after treatment. Values are shown as a ratio relative to cyclopamine 0 μmol/L. Suppression of mRNA levels of mGpr49 and mGli1 was dependent on the concentration of cyclopamine. **C:** Time course of mRNA expression of mGpr49 and mPtch1 in NIH3T3 cells treated with purmorphamine. Cells were treated with 2 μmol/L of purmorphamine for the time indicated in the figure. Ptch1 is a well-known target of HH signaling. Upregulation of mGpr49 (left) expression was dependent on the time course, as with mPtch1 (right). Statistical analysis using Pearson's coefficient was calculated for each time's combination and a high correlation was seen between the expression levels of mGpr49 and mPtch1 at $r = 0.945$ ($P < 0.01$). **D:** After transfection of mouse Gli1-expression vector to NIH3T3, mRNA levels of mGpr49 and mPtch1 were assayed at the time indicated in the figure. The ratios of mRNA level of mGli1-transfected to vector-transfected cells were estimated, and the values are shown as the ratio to the value at 0 hours. When Gli1 is expressed in NIH3T3 cells, the gene expression level of mGpr49 and mPtch1 were elevated.

mouse Gli1, a target of HH signaling,[3] and this down-regulation was dependant on the time after treatment and the concentration of cyclopamine (Figure 5A and B). Next, to see whether GPR49 expression is up-regulated by HH signaling, we treated mouse embryonic fibroblast NIH3T3 cells, which are known to respond to HH signaling, with the HH agonist purmorphamine. The expression of mouse Gpr49 was increased together with mouse Ptch1, another target of HH signaling, in a time-dependent manner (Figure 5C). Up-regulation of mouse GPR49 was also confirmed when we transfected mouse Gli1 expression vector[13] to NIH3T3 (Figure 5D). These findings indicate that GPR49 is regulated by HH signaling.

Discussion

Our studies demonstrated that GPR49 is specifically overexpressed in BCC and plays a significant role in tumor formation and cell proliferation.

DNA microarray analysis in our samples showed *GPR49* expression to be about 8.3-fold higher than normal skin. This result is reliable because our data includes almost all genes reported to be overexpressed in BCC.[3,17,18] In QRT-PCR study, GPR49 was markedly overexpressed in 19 of 20 BCC samples of nodular and superficial types in comparison with normal tissue samples. On the other hand, other types of malignant epidermal tumors did not show significant upregulation of GPR49. Together with the result of *in situ* hybridization, our study suggests that the overexpression of GPR49 is a characteristic feature of BCC. Several reports show that BCC is a tumor of hair follicle origin. In particular, follicular bulge stem cells and their progeny with high self-renewal capacity are suggested to play the role in BCC formation.[19] In support of this idea, the expression of keratin 6a, a marker of the follicular bulge stem cells[20] or their progeny,[21] was 6.8-fold higher in BCC than in normal skin in our DNA microarray analysis (data not shown). Recent report shows that GPR49 is the second most highly up-regulated gene as assessed by differential expression arraying on isolated hair follicle stem cells.[22] Together with the report that GPR49 marks stem cells in intestine and hair follicle,[7] our experiment suggest that BCC is similar to hair follicle stem cells.

Our data also showed that down-regulation of Gpr49 suppressed ASZ001 cell proliferation without inducing differentiation or apoptosis, and GPR49-overexpressing HaCaT cells showed cell proliferation *in vitro*. Furthermore, GPR49-overexpressing HaCaT cells showed tumor formation when transplanted into NOG mice. Even though the nodules of HaCaT-vector cells showed epidermal cyst-like structures on histological examination, the tumors of GPR49-overexpressing HaCaT cells showed not only nuclear atypia but also a complicated nest with cancer pearls and invasion into the stroma. Also, increased expression of Ki-67 in the tumors of GPR49-overexpressing HaCaT cells was observed. Though the tumor showed features of squamous cell carcinoma instead of BCC, this could be explained by differences in the character of the BCC progenitor cells and more highly differentiated HaCaT cells. These histological alterations by GPR49 overexpression revealed that GPR49 functions as an oncogene. A recent report showed that stem cells in the small intestine and colon overexpress GPR49, and also possibly in the hair folli-

cle.[7] But it was unclear whether GPR49 has a functional role or whether it is simply a stem cell marker. Our results show that GPR49 does have a role in cell proliferation, at least in some cell types. As discussed in the emerging concept of "cancer stem cells," some subpopulations of tumor cells possessing somatic stem cell markers have a high proliferative characteristics.[23] But this concept is somewhat controversial since this phenomenon goes against the original concept that somatic stem cells are defined as those with slow cell cycling. However, this phenomenon is now reported in various types of cancers, and the current idea is that the difference between somatic and cancer stem cells is explained by how strictly self-renewal is regulated.[23] Therefore, considering these theories, we speculate that BCC cells possess the features somewhat similar to follicular stem cells, while dysregulated expression of the stem cell marker GPR49 led to abnormal cell proliferation and tumor formation.

Some studies have also suggested that G-protein-coupled receptors are involved in carcinogenesis.[24] In particular GPR48, which is also a member of the LGRs, plays a significant role in invasion and metastasis of carcinoma cell.[25] GPR49 has potential SH2- and SH3-interacting sequences in the C-terminal tail and it may be able to link to additional signal transduction cascades. Therefore, together with our observations about functional analysis, GPR49 may be closely involved in the tumorigenesis of BCC. These data also suggested that GPR49 will be a novel target of therapy in BCC. Because a numbers of drugs currently in use are agonists or antagonists of G protein-coupled receptors, we speculate that antagonists of GPR49 will also be a drug for treating BCC. So, future studies to identify the ligand of GPR49 would be useful.

Our results indicated that gene expression of GPR49 and GLI1 showed significant correlation in BCC tumor samples. Moreover, inhibition of the HH signaling pathway in a mouse BCC cell line down-regulated endogenous Gpr49, and activation of HH signaling in mouse NIH3T3 cells up-regulated endogenous GPR49. These findings indicate that GPR49 is regulated by HH signaling. Previous reports showed that *GPR49* is regulated by Wnt-β -catenin signaling,[7,8] but our data suggested that GPR49 is also regulated by HH signaling in BCC. However, we could not find the GLI binding site or related sequences[13] in the promoter region of *GPR49*. Also, luciferase assay using reporter constructs of the *GPR49* promoter region did not show significant activity (data not shown). However, the regulation of HH signaling target genes in mammals seems complicated. For instance, GLI binding sites of *N-MYC*, which is also thought to be a target gene of HH signaling, may exist in the second intron and about 50 kb upstream of the transcription start site.[26] There may also some intermediary step exist to induce GPR49. One possibility is that GPR49 is expressed via the activation of Wnt-β catenin signaling, since past studies suggested that activation of HH signaling induces activation of Wnt-β catenin signaling.[27] However, we could not successfully prove this hypothesis in our BCC cases because immunohistochemistry of β catenin in BCC cases did not show nuclear accumulation (data not shown). And reporter activity of TOP flash/FOP flash[28] was negligible in ASZ001 in comparison with the high activity seen in hepatocellular carcinoma cells in which Wnt-β catenin signaling had been activated (data not shown). So at present, we do not know whether GPR49 is up-regulated by HH signaling directly or whether there are any intermediate steps. Further analysis is necessary to reveal the precise regulation of the gene expression.

In conclusion, stem cell marker GPR49 is expressed in BCC and plays a significant role in the pathogenesis of BCC. Because some cancer cells and tissue development share the HH signaling pathway, GPR49 might be a key molecule with roles common to both the carcinogenesis and normal tissue development pathways.

Acknowledgments

We thank Dr. Ervin Epstein (Department of Dermatology, University of California San Francisco) and Dr. Matthew P. Scott (Department of Developmental Biology, Howard Hughes Medical Institute, Stanford University School of Medicine) for providing ASZ001 cells; Norbert Fusenig (Division of Carcinogenesis and Differentiation *in vitro*, German Cancer Research Center) for providing the HaCaT cells; Dr. Hiroshi Sasaki (Laboratory for Embryonic Induction, RIKEN Center for Developmental Biology) for providing mouse Gli1 expression vector, 8×3'GBS-luc reporter and 8× mutant3'GBS-luc reporter; Dr. Toru Kiyono (Virology Division, National Cancer Center Research Institute) for providing pENTR221 vector and pDEST-SI-CMSCVpuro vector; and Drs. Syunichi Miyakawa (Department of Dermatology, Kawasaki Municipal Hospital), Shinichi Takahashi (Department of Dermatology, University of Tokyo Dental College, Ichikawa Hospital), Yasuki Hata (Department of Dermatology, Kanagawa Saiseikai Hospital), and Junki Ogawa (Department of Dermatology, Nihon Koukan Hospital) for providing samples of BCC cases.

References

1. Schirren CG, Rütten A, Kaudewitz P, Diaz C, McClain S, Burgdorf WH: Trichoblastoma and basal cell carcinoma are neoplasms with follicular differentiation sharing the same profile of cytokeratin intermediate filaments. Am J Dermatopathol 1997, 19:341–350
2. Wicking C, McGlinn E. The role of hedgehog signalling in tumorigenesis. Cancer Lett 2001, 173:1–7
3. Bonifas JM, Pennypacker S, Chuang PT, McMahon AP, Williams M, Rosenthal A, De Sauvage FJ, Epstein EH Jr: Activation of expression of hedgehog target genes in basal cell carcinomas. J Invest Dermatol 2001, 116:739–742
4. Hsu SY, Kudo M, Chen T, Nakabayashi K, Bhalla A, van der Spek PJ, van Duin M, Hsueh AJ: The three subfamilies of leucine-rich repeat-containing G protein-coupled receptors (LGR): identification of LGR6 and LGR7 and the signaling mechanism for LGR7. Mol Endocrinol 2000, 14:1257–1271
5. Hsu SY: New insights into the evolution of the relaxin-LGR signaling system. Trends Endocrinol Metab 2003, 14:303–309
6. Morita H, Mazerbourg S, Bouley DM, Luo CW, Kawamura K, Kuwabara Y, Baribault H, Tian H, Hsueh AJ: Neonatal lethality of LGR5 null mice is associated with ankyloglossia and gastrointestinal distension. Mol Cell Biol 2000, 24:9736–9743
7. Barker N, van Es JH, Kuipers J, Kujala P, van den Born M, Cozijnsen M, Haegebarth A, Korving J, Begthel H, Peters PJ, Clevers H: Identifi-

cation of stem cells in small intestine and colon by marker gene Lgr5. Nature 2007, 449:1003–1007
8. Yamamoto Y, Sakamoto M, Fujii G, Tsuiji H, Kenetaka K, Asaka M, Hirohashi S: Overexpression of orphan G-protein-coupled receptor, Gpr49, in human hepatocellular carcinomas with βcatenin mutations Hepatology 2003, 37:528–533
9. McClanahan T, Koseoglu S, Smith K, Grein J, Gustafson E, Black S, Kirschmeier P, Samatar AA: Identification of Orphan G protein-coupled receptor GPR49 in human colon and ovarian primary tumors. Cancer Biol Ther 2006, 5:419–426
10. Scharffetter K, Lankat-Buttgereit B, Kreig T: Localization of collagen mRNA in normal and scleroderma skin by in-situ hybridization. Eur J Clin Invest 1998, 18:9–17
11. Jin W, Kim BC, Tognon C, Lee HJ, Patel S, Lannon CL, Maris JM, Triche TJ, Sorensen PH, Kim SJ: The ETV6-NTRK3 chimeric tyrosine kinase suppresses TGF-beta signaling by inactivating the TGF-beta type II receptor. Proc Natl Acad Sci USA 2005, 102:16239–16244
12. Xie J, Aszterbaum M, Zhang X, Bonifas JM, Zachary C, Epstein E, McCormick F: A role of PDGFRα in basal cell carcinoma proliferation. Proc Natl Acad Sc 2001, 98:9255–9259
13. Sasaki H, Hui C, Nakafuku M, Kondoh H: A binding site for Gli proteins is essential for HNF-3beta floor plate enhancer activity in transgenics and can respond to Shh in vitro. Development 1997, 124:1313–1322
14. Brummelkamp TR, Bernards R, Agami R: A system for stable expression of short interfering RNAs in mammalian cells. Science 2002, 296:550–553
15. Aszterbaum M, Epstein J, Oro A, Douglas V, LeBoit PE, Scott MP, Epstein EH Jr: Ultraviolet and ionizing radiation enhance the growth of BCCs and trichoblastomas in patched heterozygous knockout mice. Nat Med 1999, 5:1285–1291
16. Boukamp P, Petrussevska RT, Breitkreutz D, Hornung J, Markham A, Fusenig NE: Normal keratinization in a spontaneously immortalized aneuploid human keratinocyte cell line. J Cell Biol 1988, 106:761–771
17. Eichberger T, Regl G, Ikram MS, Neill GW, Philpott MP, Aberger F, Frischauf AM: FoxE1, A new transcriptional target of GLI2, is expressed in human epidermis and basal cell carcinoma J Invest Dermatol 2004, 122:1180–1187
18. Cui C, Elsam T, Tian Q, Seykora JT, Grachtchouk M, Dlugosz A, Tseng H: Gli proteins up-regulate the expression of basonuclin in basal cell carcinoma. Cancer Res 2004, 64:5651–5658
19. Mancuso M, Leonardi S, Tanori M, Pasquali E, Pierdomenico M, Rebessi S, Di Majo V, Covelli V, Pazzaglia S, Saran A: Hair cycle-dependent basal cell carcinoma tumorigenesis in Ptc1neo67/+ mice exposed to radiation. Cancer Res 2006, 66:6606–6614
20. Tumbar T, Guasch G, Greco V, Blanpain C, Lowry WE, Rendl M, Fuchs E: Defining the epithelial stem cell niche in skin. Science 2004, 16:303:359–363
21. Gu LH, Coulombe PA: Keratin expression provides novel insight into the morphogenesis and function of the companion layer in hair follicles. J Invest Dermatol 2007, 127:1061–1073
22. Morris RJ, Liu Y, Maries L, Yang Z, Trempus C, Li S, Lin JS, Sawicki JA, Cotsarelis G: Capturing and profiling adult hair follicle stem cells. Nature Biotechnol 2004, 22:411–417
23. Spillane JB, Henderson MA: Cancer stem cells: a review. ANZ J Surg 2007, 77:464–468
24. Li S, Huang S, Peng SB: Overexpression of G protein-coupled receptors in cancer cells: involvement in tumor progression. Int J Oncol 2005, 27:1329–1339
25. Gao Y, Kitagawa K, Hiramatsu Y, Kikuchi H, Isobe T, Shimada M, Uchida C, Hattori T, Oda T, Nakayama K, Nakayama KI, Tanaka T, Konno H, Kitagawa M: Up-regulation of GPR48 induced by down-regulation of p27Kip1 enhances carcinoma cell invasiveness and metastasis. Cancer Res 2006, 66:11623–11631
26. Hallikas O, Palin K, Sinjushina N, Rautiainen R, Partanen J, Ukkonen E, Taipale J: Genome-wide prediction of mammalian enhancers based on analysis of transcription-factor binding affinity. Cell 2006, 124:47–59
27. Boonchai W, Walsh M, Cummings M, Chenevix-Trench G: Expression of beta-catenin, a key mediator of the WNT signaling pathway, in basal cell carcinoma. Arch Dermatol 2000, 136:937–938
28. Coghlan MP, Culbert AA, Cross DA, Corcoran SL, Yates JW, Pearce NJ, Rausch OL, Murphy GJ, Carter PS, Roxbee Cox L, Mills D, Brown MJ, Haigh D, Ward RW, Smith DG, Murray KJ, Reith AD, Holder JC: Selective small molecule inhibitors of glycogen synthase kinase-3 modulate glycogen metabolism and gene transcription. Chem Biol 2000, 7:793–803

Modern Pathology (2008) 21, 992–1001

www.modernpathology.org

Histopathological features and prognostic significance of the micropapillary pattern in lung adenocarcinoma

Kazunori Kamiya[1,2], Yuichiro Hayashi[1], Junya Douguchi[1], Akinori Hashiguchi[1], Taketo Yamada[1], Yotaro Izumi[2], Masazumi Watanabe[2], Masafumi Kawamura[2], Hirohisa Horinouchi[2], Naoki Shimada[3], Koichi Kobayashi[2] and Michiie Sakamoto[1]

[1]*Department of Pathology, School of Medicine, Keio University, Tokyo, Japan;* [2]*Department of Surgery, Division of General Thoracic Surgery, School of Medicine, Keio University, Tokyo, Japan and* [3]*Department of Preventive Medicine and Public Health, School of Medicine, Keio University, Tokyo, Japan*

The micropapillary pattern is characterized by small papillary tufts with no fibrovascular core lying in spaces and has been reported as an aggressive variant of carcinoma in several organs. We investigated the histopathobiological properties of the micropapillary pattern with immunohistochemistry, serial sections, and electron microscopy in lung adenocarcinoma. We further analyzed its clinicopathological character and prognosis. The subjects included 383 adenocarcinoma cases, of which 184 (48%) were micropapillary pattern-positive and 199 (52%) were micropapillary pattern-negative. On histology, micropapillary tufts seemed to float in the alveolar space or spaces encased by connective tissues, whereas serial sections revealed that most tufts had continuity with other tufts and even with the main tumor. Positive staining for the adhesion molecules E-cadherin and β-catenin suggested the preservation of tight adhesion, and electron microscopy showed the existence of intercellular junctions. Negative staining for laminin and loss of basement membrane as determined by electron microscopy suggest a loss of cell–matrix contact. Positive staining for Ki-67 indicates that cells constituting micropapillary tufts retained their proliferation potency. There were no CD34-positive cells in micropapillary tufts, and the loss of the vascular core was confirmed. In micropapillary pattern-positive cases, lymphatic invasion was identified significantly more frequently than in micropapillary pattern-negative cases ($P<0.001$), even at stageIA (without lymph node metastasis, $N=197$) ($P<0.001$). The 5-year and 10-year overall survival rates of the micropapillary pattern-positive stageIA group were 77.6 and 67.6%, respectively, which were significantly less than those of the micropapillary pattern-negative stageIA group (98.1 and 98.1%) ($P=0.001$). In conclusion, cells constituting the micropapillary pattern are likely to have acquired anchorage-independent growth and a potential for high malignancy.
Modern Pathology (2008) **21**, 992–1001; doi:10.1038/modpathol.2008.79; published online 30 May 2008

Keywords: lung adenocarcinoma; micropapillary pattern; histopathology; prognosis; immunohistochemistry; electron microscopy

Introduction

Lung cancer is one of the most common causes of cancer-related death worldwide.[1] The prognosis of patients with lung cancer is generally poor, and the overall 5-year survival rate is 15%.[2] Of the four main histological types of lung cancer, adenocarcinoma is increasing in frequency and accounts for almost half of all lung cancers.[3] Recent advances in diagnostic imaging have enhanced the capability for diagnosis at the early stage, and histopathological studies indicate the existence of good prognostic groups in lung cancer. Bronchioloalveolar carcinoma, defined as a non-invasive subtype of lung adenocarcinoma,[3] is recognized as ground-glass opacity lesion on computed tomography and is reported to have a good prognosis.[4] However, the overall 5-year survival of patients with stageIA (T1N0M0: T1, tumor greatest dimension ≤30 mm and surrounded by pleura; N0, no regional lymph node metastasis; M0, no distant metastasis)[5] adenocarcinomas does not reach 80%,[6,7] which indicates the existence of a poor prognostic group. Factors including smoking history, serum level of carcinoembryonic antigen, and tumor size, as well as lymphatic and venous

Correspondence: Dr M Sakamoto, MD, Department of Pathology, School of Medicine, Keio University, 35 Shinano-machi, Shinjyuku-ku, Tokyo 160-8582, Japan.
E-mail: msakamot@sc.itc.keio.ac.jp
Received 03 January 2008; revised 16 April 2008; accepted 17 April 2008; published online 30 May 2008

invasion have been identified as poor prognostic factors for lung adenocarcinoma.[8–12]

Recently, a pathological entity called the micropapillary pattern has been reported to have worse outcomes in breast,[13] colon,[14] urinary tract,[15] ovary,[16] salivary gland,[17] and lung[18,19] cancer. The micropapillary pattern in lung adenocarcinoma is characterized by small papillary tufts lying in alveolar spaces or in spaces encased by connective tissues, with the tufts having no fibrovascular core,[18,19] and it has been reported as an important factor for poor prognosis.[18–21] However, the detailed histopathobiological features of the micropapillary pattern have not yet been clarified. We investigated the histological, immunohistochemical, electron microscopic, and clinicopathological properties of the micropapillary pattern to elucidate why it could be a factor in poor prognoses.

Materials and methods

Surgical Specimens and Patient Characteristics

From January 1993 to December 2006 in Keio University Hospital, 526 patients underwent complete surgical resection of lung cancer diagnosed as primary lung adenocarcinoma. We reviewed these sections macroscopically and microscopically as mentioned below. The histological type of the tumor was described according to the World Health Organization classification[3] and pathological staging was performed according to the classification of the Union Internationale Coutre le Cancer.[5] Because bronchioloalveolar carcinoma has been defined as a non-invasive lesion[3] and there was no existence of the micropapillary pattern in cases composed only of bronchioloalveolar carcinoma ($N=68$), we excluded these cases from clinicopathological analysis. For accuracy of survival analysis, stageIIIB and stageIV cases with the possibility of incomplete resection were excluded as well. Therefore, the final population for clinicopathological analysis consisted of 383 cases (214 men and 169 women ranging from 29 to 85 years of age, with an average age of 62.3 years). Clinicopathological information was obtained by reviewing the medical charts in detail with regard to age (<60 or ≥ 60 years), sex (male or female), smoking history (nonsmoker or smoker: smoker was defined as more than 1 year of smoking history), recurrence, and survival. The follow-up period ranged from 3 to 158 months (mean was 60.9 months). This study was conducted under the approval of the Ethics Committee of the Keio University School of Medicine.

Histological Examination

Surgically resected specimens were fixed routinely in 10% formalin, cut serially into 5- to 7-mm-thick slices, and macroscopically examined. From the section including the maximum tumor diameter, all the tumor tissues as well as the surrounding lung tissue were removed and embedded in paraffin, and then cut into 4-μm-thick sections. Finally, hematoxylin–eosin and Elastica Van Gieson staining were performed and all sections for each patient were observed. The following histopathological factors were evaluated: tumor size (maximum tumor diameter ≤ 30 or >30 mm), lymph node metastasis, pleural invasion, lymphatic invasion, and venous invasion. The histological patterns were divided into four distinctive subtypes: bronchioloalveolar carcinoma as well as acinar, papillary, and solid adenocarcinoma with mucin; the latter three subtypes were defined as invasive.[3] The dominant subtype of each tumor was then documented.

The micropapillary pattern was defined according to the two previous studies;[18,19] it was identified as small tufts lying in alveolar spaces or in spaces encased within thin walls of connective tissue, and the tufts had no fibrovascular core. The extent of the micropapillary pattern was subclassified as none (0% of the tumor), focal ($<10\%$), moderate ($<50\%$), or extensive ($\geq 50\%$) based on the proportion of micropapillary pattern area in the tumors.

Furthermore, three micropapillary pattern-positive samples (extent: moderate and extensive) were selected and 100 serial sections stained by hematoxylin–eosin were then examined sequentially at intervals of 12 μm with attention paid to the morphology of the micropapillary pattern.

Immunohistochemistry

For immunohistochemistry, 20 cases of tumor with the micropapillary pattern were randomly selected and studied (10 cases with lymph node metastasis and 10 without).

Four-micrometer-thick sections were deparaffinized, rehydrated, and incubated in 0.03% H_2O_2 in 95% methanol at room temperature for 20 min to block the endogenous peroxidase activity. Autoclave pretreatment at 120°C for 10 min in 10 mM citrate buffer (pH 6.0) was used for E-cadherin and Ki-67 antigen retrieval. Water bath pretreatment at 100°C for 10 min in 10 mM citrate buffer (pH 9.0) was used for β-catenin and CD34 antigen retrieval. Incubation in 4 mg/ml pepsin (Dako, Glostrup, Denmark) in 0.2 N HCl at 37°C for 60 min was used for laminin antigen retrieval. All sections were incubated for 20 min with normal horse serum to eliminate nonspecific staining and then incubated with the following primary antibodies: anti-human E-cadherin (1:200; Novocastra Laboratories, Newcastle, UK), anti-human β-catenin (1:200; Santa Cruz Technology, Santa Cruz, CA, USA), anti-human laminin (1:400; Dako), anti-human CD34 (1:100, Dako), and anti-human Ki-67 (diluted at 1:400; Dako). These antibodies were applied overnight at 4°C, followed by incubation with the secondary antibody